

Chapter 2

Photoelectrochemical Behavior of *n*-GaAs in Acetonitrile Solutions

1. Introduction

The photoelectrochemical behavior of GaAs/liquid contacts has attracted much attention in attempts to compare theoretical predictions with the experimental behavior of semiconductor electrodes.¹⁻¹⁶ There has been significant controversy regarding the electron-transfer rate constant, k_{et} , at semiconductor/liquid interfaces. While many experimental results and theoretical studies have indicated that the upper bounds on k_{et} is on the order of 10^{-17} to 10^{-16} cm^4s^{-1} ,^{4,9-11,15-17} other reports have suggested that k_{et} can be as large as 10^{-12} to 10^{-10} cm^4s^{-1} .^{7,18-20} Steady-state current density (J) vs. potential (E) data obtained on n -GaAs/ CH_3CN -cobaltocenium-cobaltocene (CoCp_2)⁺⁰ contacts in the limit where the observed rate does not exhibit the expected second-order rate law (first order in the surface electron concentration and first order in the redox acceptor concentration) have been interpreted to indicate that k_{et} values at semiconductor/liquid contacts can be as high as 10^{-10} cm^4s^{-1} .⁷ Subsequent reports on n -GaAs/ CH_3CN contacts have relied upon solvent-suspended quartz crystal microbalance measurements to indicate that both cobaltocene and cobaltocenium adsorb onto the GaAs surface.⁸ Assumptions about the effective electron-transfer distance to the adsorbed species, the distance-dependence of the orbital coupling overlap, and the surface coverage of adsorbed electroactive species in this system have then yielded a 10,000-fold reduction in the inferred k_{et} value to $k_{et} \approx 10^{-14}$ cm^4s^{-1} .^{7,8}

It is therefore of great interest and importance to examine in detail the J - E properties of the n -GaAs/ CH_3CN interface. The behavior of n -GaAs in contact with CH_3CN has been studied previously by a number of workers. Wrighton and Bard used cyclic voltammetry techniques to conclude that Fermi-level pinning was present at n -GaAs/ CH_3CN contacts over a wide range of redox potentials.²¹ Nagasubramanian, Wheeler and Bard subsequently reached identical conclusions based on impedance

measurements of n -GaAs/CH₃CN contacts.²² Other studies indicating non-ideal junction behavior of n -GaAs electrodes in propylene carbonate, tetrahydrofuran, dimethylformamide, and aluminum chloride-butylpyridinium chloride molten salt electrolyte systems have been reported.²³⁻³¹ Reduction of the influence of surface states has, in certain cases, resulted in efficient GaAs-based photoelectrochemical cells, specifically for n -GaAs/CH₃CN-ferricenium-ferrocene (Fc⁺⁰) contacts.^{32,33}

While J - E behaviors of n -GaAs/CH₃CN contacts with a series of metallocenes have been studied previously in our laboratory, the focus of this chapter involves the investigation of the photoelectrochemical properties of n -GaAs/CH₃CN-cobaltocenium-cobaltocene (CoCp₂⁺⁰) contacts. The presence of Fermi-level pinning is confirmed by correlating the barrier height obtained for this junction with prior results. This chapter also presents a series of experiments designed to probe the presence of irreversible chemical and/or electrochemical changes on GaAs electrodes during electrochemical process in CH₃CN-CoCp₂⁺⁰ solution. These results display the non-ideal behavior of n -GaAs/CH₃CN-CoCp₂⁺⁰ junction and consequently the invalidity of k_{et} extraction using the J - E data from this system.

2. Background

2.1. Determination of the Electron-Transfer Rate Constant at the Semiconductor/Liquid Interface

Current density vs. potential (J - E) measurements, in conjunction with kinetic information obtained from impedance measurements, can be useful tools for assessing the electron-transfer rate constants, k_{et} at semiconductor/liquid interfaces. In order to extract robust k_{et} values from the steady-state J - E data, the following three conditions must be satisfied.

(1) The electron transfer from the conduction band of a semiconductor to an outer sphere redox acceptor in solution must follow a second-order rate law given by

$$-\frac{d[A]}{dt} = k_{\text{et}}n_s[A] \quad (2.1)$$

where n_s is the concentration of surface electrons in the conduction band, and $[A]$ is the concentration of redox acceptors located near the surface of the semiconductor. The interfacial flux must be shown to be first order in the n_s at the semiconductor surface and first order in the $[A]$ in the solution.^{4,34} In this case, interfacial electron transfer dominates the recombination current, and $J_0 = qk_{\text{et}}n_s[A]$. By varying the concentration of redox acceptors, V_{oc} should change accordingly.

A prior study of n -GaAs/CH₃CN-Fc⁺⁰ contacts in our laboratory had shown that a change of two orders of magnitude of $[A]$ and $[A^-]$, while the solution potential remained constant, produced no change in V_{oc} value at a constant light intensity. There was also no change in V_{oc} at a constant photocurrent density as $[A]$ was increased from 0.5 mM to 33.4 mM while $[A^-]$ remained constant.³⁵ This result clearly demonstrated that the

variation in $[A]$ did not affect the interfacial flux, and therefore interfacial electron transfer current does not dominate the recombination current.

(2) The semiconductor band edges do not move with changes in the concentration of the redox acceptor species. Otherwise, the validation of the rate law is hindered when both variables of the rate law, n_s and $[A]$, are simultaneously changed.

If the band edges stay at the same positions when the redox potential is varied, then the barrier height of the junction, which is the difference between the semiconductor conduction band edge and the solution redox potential, should change linearly with the changes in the redox potential of the contacting solution. When this relationship is not observed, the junction is Fermi-level pinned, and the band edges could shift with changes in the cell potential. A prior investigation on Fermi-level pinning at n -GaAs/CH₃CN junctions was conducted by measuring the V_{oc} values at different cell potentials,³⁵ and is presented in section 2.2 of this chapter. Although the relationship between the V_{oc} and the cell potential can provide an indication for the degree of Fermi-level pinning, the observed changes in V_{oc} could also be caused by reasons other than the band edge movement. For example, the interfacial electron transfer current could increase with changes in the equilibrium barrier height at the interface, or the surface-state recombination current could have increased due to the changes in equilibrium occupation fraction of the surface states. Since these conditions are capable of affecting the measured V_{oc} values as well, the barrier height measurement would be essential for confirming the presence of Fermi-level pinning.

(3) The capture of the electrons by surface states does not compete kinetically with the direct electron transfer from the semiconductor to the redox acceptor species.^{4,34,36-39} The surface states can either be intrinsic or arise from adsorption of the redox species. If the semiconductor surface reacts with the contacting solution, it is a good indication that the surface-state process dominates the interfacial kinetics.

The investigation of *n*-GaAs surface reaction in contact with CH₃CN-CoCp₂⁺⁰ is one of the main focuses of this chapter. The V_{oc} of this junction was larger than expected at such a negative cell potential, which is fairly close to the GaAs conduction band edge. If the GaAs surface is modified during the electrochemical operation in this solution, the extraction of k_{et} value from the steady-state $J-E$ data of this junction would certainly not be possible.

2.2. Fermi-Level Pinning

In an ideal situation, a change in the redox potential of the solution should result in a defined change in the barrier height (ϕ_b) of the junction; however, this behavior is not always observed experimentally. When a reliable barrier height measurement technique was unavailable, open-circuit photovoltages, V_{oc} , were measured and related to the thermodynamic quantities for the investigation of the Fermi-level pinning. For an *n*-type semiconductor when the interfacial electron transfer is the dominating recombination process, V_{oc} can be related to the build-in voltage (V_{bi}) according to the equation:

$$V_{oc} = \frac{kT}{q} \ln\left(\frac{J_{ph}}{qN_c k_{et}[A]}\right) + V_{bi} \quad (2.2)$$

However, if the interfacial electron transfer current is much less than the total recombination current, then the inequality in Equation 2.2 must hold. Since $\phi_b = V_{bi} + (kT/q)\ln(N_c/N_d)$, V_{oc} can be related to ϕ_b as follows:

$$V_{oc} < \frac{kT}{q} \ln\left(\frac{J_{ph}}{qN_c k_{et}[A]}\right) + \phi_b \quad (2.3)$$

The electrochemical behavior of a series of *n*-GaAs/CH₃CN contacts has been investigated over a significant range of Nernstian solution potentials, $E(A/A^-)$, in order to

ascertain whether “ideal” behavior of the V_{oc} vs. $E(A/A^-)$ is observed for these contacts, or whether Fermi-level pinning, which would lead to apparent band edge shifts as $E(A/A^-)$ is changed,²¹ is present in these systems. The former condition is required for a straightforward extraction of k_{et} values from $J-E$ data, while, in contrast, the latter behavior has been observed in prior cyclic voltammetry and impedance measurements of n -GaAs/CH₃CN contacts.^{22,40-42}

Several different metallocene-based redox couples, spanning a wide range of formal potentials, $E^0(A/A^-)$, were used to produce a variation in the Nernstian potentials of the electrolyte solutions from -1.2 V to $+0.2$ V vs. SCE. Figure 2.1 displays the V_{oc} of each system recorded at a light intensity sufficient to provide a photocurrent density of 1 mA cm⁻² at each n -GaAs/CH₃CN contact. Despite a change of over 1.2 V in $E(A/A^-)$ between the n -GaAs/CH₃CN-Co(C₅H₄CH₃)₂⁺⁰ and the n -GaAs/CH₃CN-Fc⁺⁰ contacts, the V_{oc} only changed by ~ 0.3 V.⁴³ In the ideal model of semiconductor photoelectrochemistry, the V_{oc} should be linearly dependent on $E(A/A^-)$, with a slope close to unity, for a homologous series of redox species. Instead, a much weaker dependence of V_{oc} was observed as $E(A/A^-)$ was varied, and the presence of Fermi-level pinning in this system over the range of potentials investigated was indicated. Furthermore, for $E(A/A^-)$ more negative than -0.80 V vs. SCE, the measured V_{oc} values that are larger than expected from the linear region signals the possibility of a chemical reaction between the n -GaAs and CH₃CN-based electrolyte under the conditions explored.

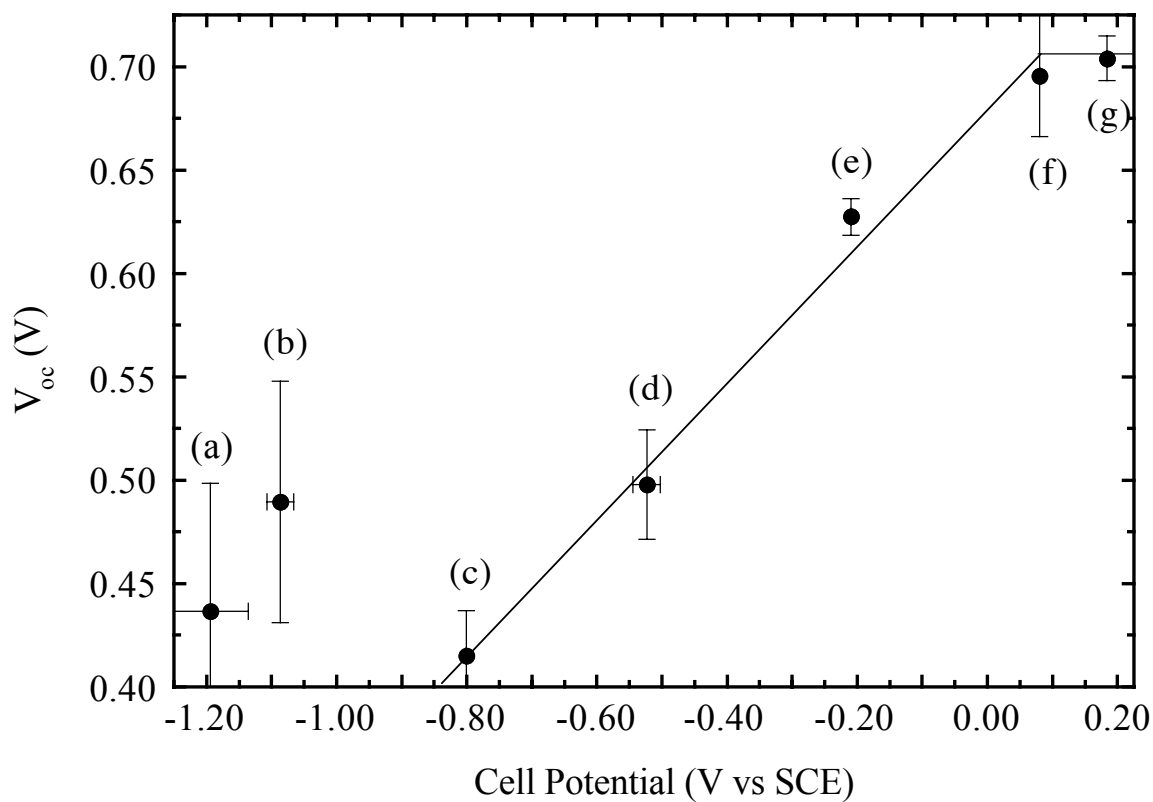


Figure 2.1

Open-circuit photovoltage vs. equilibrium cell potential for the *n*-GaAs/CH₃CN-LiClO₄

system at $J_{ph} = 1.0 \text{ mA cm}^{-2}$. The redox couples used for this system are (a)

Co(C₅H₄CH₃)₂⁺⁰, (b) CoCp₂⁺⁰, (c) [CoCp(C₅H₄CO₂CH₃)]⁺⁰, (d) Co(C₅H₄CO₂CH₃)₂⁺⁰, (e)

Fe[C₅(CH₃)₅]₂⁺⁰, (f) Fe(C₅H₄CH₃)₂⁺⁰, (g) FeCp₂⁺⁰.⁴³

3. Experimental

3.1. Electrode Material and Etching

Single-crystal Si-doped (100)-oriented *n*-GaAs (Laser Diode Co.) with dopant density, N_d , of $(0.9\text{--}1.9) \times 10^{17} \text{ cm}^{-3}$ and wafer thickness of 400–500 μm were used. Ohmic contacts were prepared by thermal evaporation of a 1000 Å layer of 98% Au:2% Ge alloy (Alfa Aesar) or 88% Au:12% Ge alloy (Aesar) on the unpolished side of the wafers, followed by annealing in forming gas at 475 °C for 5 minutes.³³ Electrodes were fabricated by attaching a tinned copper wire (22 AWG, Belden) to the ohmic contact using electrically conductive silver print (GC Electronics). The wire was encased in glass tubing and the backside and edges of the electrode were sealed with insulating white epoxy (Epoxy Patch Kit 1C, Dexter Corp.), leaving only the polished surface of the crystal exposed. Electrode areas were determined by digitizing magnified scanned images of the electrode along with a micro ruler using ImageSXM program. The typical exposed electrode areas were 0.15–0.25 cm^2 .

For surface x-ray photoelectron spectroscopy (XPS) studies, either 2 mm × 4 mm size samples or electrodes with surface areas of 0.10–0.15 cm^2 were used. To investigate the surface property of GaAs following the electrochemical measurements, the length of the electrode glass tubing had to be reduced before it could be brought into the ultrahigh vacuum (UHV) system for XPS analysis. Prior to electrochemical experiments, the glass tubing that encases the tinned copper wire was pre-cut at ~1 inches from the epoxy and reconnected with heat-shrink tubing. The upper part of the glass tubing can then be easily removed after the electrochemical experiment by cutting away the heat-shrink tubing. With the wire folded back, the electrode can be mounted onto a stub and introduced into the UHV chamber. For some electrodes the glass tubing was replaced

with flexible polyethylene tubing, and the wire encased in polyethylene tubing can be folded back so the length of the electrode is less than 1.5 inches. These electrodes could be reused for electrochemical experiments by either unfolding the wire and reconnecting the glass tubing or unfolding the polyethylene tubing.

The *n*-GaAs working electrodes were initially etched in a 4:1:1 H₂SO₄(aq):H₂O₂ (30%):H₂O solution, rinsed with 18.0 MΩ·cm resistivity H₂O (obtained from a Barnstead Inc. Nanopure water purification system) and CH₃CN, and dried under flowing N₂(g) before being taken into the N₂(g)-purged glove box. This oxidizing etch is known to remove ~1 μm of wafer thickness per minute.⁴³ Between experiments, the electrode surfaces were etched in a solution of 0.05% (v/v) Br₂ (EM Science) in CH₃OH (EM Science) followed by immersion in a 4.0 M solution of NH₃ in CH₃OH, which was prepared by bubbling NH₃(g) through CH₃OH until the desired concentration was achieved. The etching cycle was repeated three times, rinsed again in CH₃OH, and dried with N₂(g).^{44,45} This procedure has been shown to give an oxide free stoichiometric surface with a mirror finish.^{32,46,47}

3.2. Solvents and Reagents

Methanol (CH₃OH) and acetonitrile (CH₃CN) were obtained from EM Science or Aldrich. The CH₃OH was distilled over magnesium turnings prior to use. The CH₃CN was predried over CaH₂ and then dried over P₂O₅ and stored over activated 3 Å sieves (EM Science). Both solvents were distilled, collected and stored under N₂(g). Ferrocene (Fc, Aldrich) and cobaltocene (CoCp₂, Strem or Aldrich) were sublimed *in vacuo*. Ferrocenium tetrafluoroborate (FcBF₄) was purchased from Aldrich or prepared as previously described,⁴⁸ and was dried *in vacuo* at room temperature before use. Cobaltocenium hexafluorophosphate (CoCp₂PF₆) was purchased from Aldrich or prepared via the method of Sheats and Rausch,⁴⁹ and was recrystallized from CH₃CN and

dried *in vacuo* at room temperature. Lithium perchlorate (LiClO_4 , Aldrich or J.T. Baker) was dried by fusing at $280\text{ }^\circ\text{C}$ under active vacuum in a quartz tube.⁵⁰ All solid reagents were stored and weighed out in a $\text{N}_2(\text{g})$ -purged drybox until use.

3.3. Electrochemical Measurements

A standard three-electrode potentiostatic setup was used for all electrochemical measurements. The reference electrode was a Pt wire poised at the Nernstian solution potential, and the counter electrode was a Pt gauze of area at least 10 times larger than that of the working electrode. Both Pt reference and counter electrodes were cleaned by immersion in a 3:1 (v/v) solution of concentrated $\text{HCl}(\text{aq})$ (EM Science) and concentrated $\text{HNO}_3(\text{aq})$ (EM Science) prior to being taken into the $\text{N}_2(\text{g})$ -purged glove box. Typical cell solutions for $n\text{-GaAs}/\text{CH}_3\text{CN}\text{-CoCp}_2^{+/0}$ studies consist of 10mM CoCp_2 , 10 mM CoCp_2PF_6 , and 0.7 M LiClO_4 in CH_3CN . Typical cell solutions for $n\text{-GaAs}/\text{CH}_3\text{CN}\text{-Fc}^{+/0}$ studies consist of 90 mM Fc, 0.5 mM FcBF_4 , and 0.7 M LiClO_4 in CH_3CN . The cell solutions were magnetically stirred, and the cell potential was periodically measured relative to a methanoic SCE. All electrochemical experiments were carried out in a $\text{N}_2(\text{g})$ -purged glove box that had less than 10 ppm of O_2 as verified by the lack of fuming of $(\text{CH}_3\text{CH}_2)_2\text{Zn}$.

3.3.1. Impedance Measurements

The impedance measurements were performed on a Schlumberger Instruments Model 1260 impedance/gain-phase analyzer equipped with a Solartron 1286 Electrochemical Interface. A 10 mV ac signal with a frequency sweep from 100 Hz to 100 kHz was superimposed upon a reverse dc bias stepped in 50 mV intervals between 0.4 and 1.0 V vs. Nernstian solution potential, $E(\text{A}/\text{A}^-)$. The impedance analyzer measures the total impedance, Z , and the phase angle, θ , between Z and the input ac

signal. The real and imaginary components of the impedance, Z_{re} and Z_{im} , respectively, can then be calculated using the relationships $Z_{re} = Z \cos\theta$ and $Z_{im} = Z \sin\theta$.

The impedance data were fit to an equivalent circuit consisting of a resistor, R_s , representing the resistive loss across cell solution and lead, in series with a parallel circuit containing a differential capacitance of the semiconductor space-charge region, C_{sc} , and a space-charge resistance, R_{sc} , representing resistance to Faradaic charge transfer (Figure 2.2). This model assumes that the measured differential capacitance, C_{diff} , equals C_{sc} . The differential capacitance was computed from the impedance data using the equation:⁵¹

$$2\pi f C_{diff} = \frac{1 + \sqrt{1 - 4Z_{im}^2 / R_{sc}^2}}{2Z_{im}} \quad (2.4)$$

where f is the frequency of the ac signal and Z_{im} is the imaginary part of the measured impedance at the dc bias of interest. The R_{sc} value at each dc bias was extracted from the circular fit of the Nyquist plot. A Nyquist plot is a plot of Z_{im} vs. Z_{re} that shows the branching between these two components of the measured impedance as a function of f . At a high frequency, the effective impedance of the capacitor is small relative to R_{sc} and the C_{sc} 's contribution to Z_{im} falls to zero. As most of the current flows through the C_{sc} pathway, the observed impedance is simply R_s . At a low frequency, the effective impedance of the capacitor is high relative to R_{sc} , therefore most of the current flows through the R_{sc} pathway, and the observed impedance is $R_{sc} + R_s$. In the intermediate-frequency range, the changes in frequency translate directly into the changes in the effective impedance of the capacitor, therefore the magnitude of Z is dictated by C_{sc} . The differential capacitance measurements were performed in this capacitive frequency regime where the Faradaic charge transfer pathway is suppressed.

The differential space-charge capacitance was then related to the built-in voltage V_{bi} of the semiconductor/liquid junction by the Mott-Schottky equation:³⁴

$$C_{sc}^{-2} = \frac{2}{qN_d\epsilon\epsilon_0A_s^2} \left(E + V_{bi} - \frac{kT}{q} \right) \quad (2.5)$$

where ϵ is the dielectric constant of the semiconductor, ϵ_0 is the permittivity of free space, N_d is the semiconductor dopant density, A_s is the electrode surface area, E is the applied dc potential. By plotting C_{diff}^{-2} vs. E (i.e., a Mott-Schottky plot) for each frequency and extrapolating the linear regression of these data points to infinite capacitance, the V_{bi} of the solid/liquid junction was calculated. To assess the validity of the equivalent circuit model used in this experiment, the measured semiconductor dopant density was computed from the slope of the linear fit of C_{diff}^{-2} vs. E and compared to the value specified by the manufacturer. Only electrodes which exhibited linear Mott-Schottky plots ($R^2 \geq 0.999$, where R is the correlation coefficient) and had measured dopant densities within the range specified by the manufacturer were included in the analysis. Electrodes that yielded nonlinear or frequency-dependent plots were considered defective.

3.3.2. Steady-State Current Density vs. Potential Characteristics

Current density vs. potential (J - E) measurements were performed using a Solartron Model 1287 potentiostat or an EG&G Princeton Applied Research (PAR) Model 173 potentiostat/galvanostat equipped with an EG&G PAR Model 175 universal programmer. When EG&G PAR Model 173 potentiostat/galvanostat was used, traces were recorded on a Houston Instruments Omnigraphic 2000 recorder at a scan rate of 50 mV s⁻¹. Light intensities were controlled by the use of a 300 W ENH-type tungsten-halogen bulb in conjunction with neutral density filters (Hoya Optics). Open-circuit voltages (V_{oc}) were obtained with the sample held at open-circuit, and photocurrents (I_{ph}) were obtained with the samples held at 0.4 V vs. the cell potential $E(A/A^-)$. Photoresponse measurements were performed for both both n -GaAs/CH₃CN-CoCp₂⁺⁰ and n -GaAs/CH₃CN-Fc⁺⁰ junctions. The values of V_{oc} and J_{ph} were collected at different

light intensities by reading the appropriate quantities through a Fluke 27 digital multimeter. The diode quality factors (γ) and the reverse saturation current density (J_0) were extracted using the equation:⁵²

$$V_{oc} = \frac{\gamma k T}{q} \ln \left(\frac{J_{ph}}{J_0} \right) \quad (2.6)$$

where k is Boltzmann's constant, T is the temperature, and q is the charge on the electron.

The J - E characteristics of both n -GaAs/CH₃CN-CoCp₂⁺⁰ and n -GaAs/CH₃CN-Fc⁺⁰ systems were collected mainly to confirm the reproducibility of results from prior studies in the Lewis group. Before and after each impedance measurement, the J - E data were obtained to verify that the properties of the electrode remained unchanged over the time scale of the impedance study. To investigate the possibility of surface change during the electrochemical experiments of n -GaAs in CH₃CN-CoCp₂⁺⁰ solution, the J - E data of an n -GaAs/CH₃CN-Fc⁺⁰ contact before and after potential scans in CH₃CN-CoCp₂⁺⁰ solution were also collected. This experiment was performed in an attempt to observe any effect on the J - E properties of n -GaAs after electrochemical measurements in contact with CH₃CN-CoCp₂⁺⁰ solution. An etched n -GaAs electrode was first immersed in CH₃CN-Fc⁺⁰ solution and a series of J - E curves were recorded in the dark and at five different light intensities. The electrode was rinsed with CH₃CN before exposing to CH₃CN-CoCp₂⁺⁰ solution where three types of potential scans were performed to age the electrode. Following another CH₃CN rinse, the electrode was returned to the CH₃CN-Fc⁺⁰ solution and another series of J - E curves were obtained.

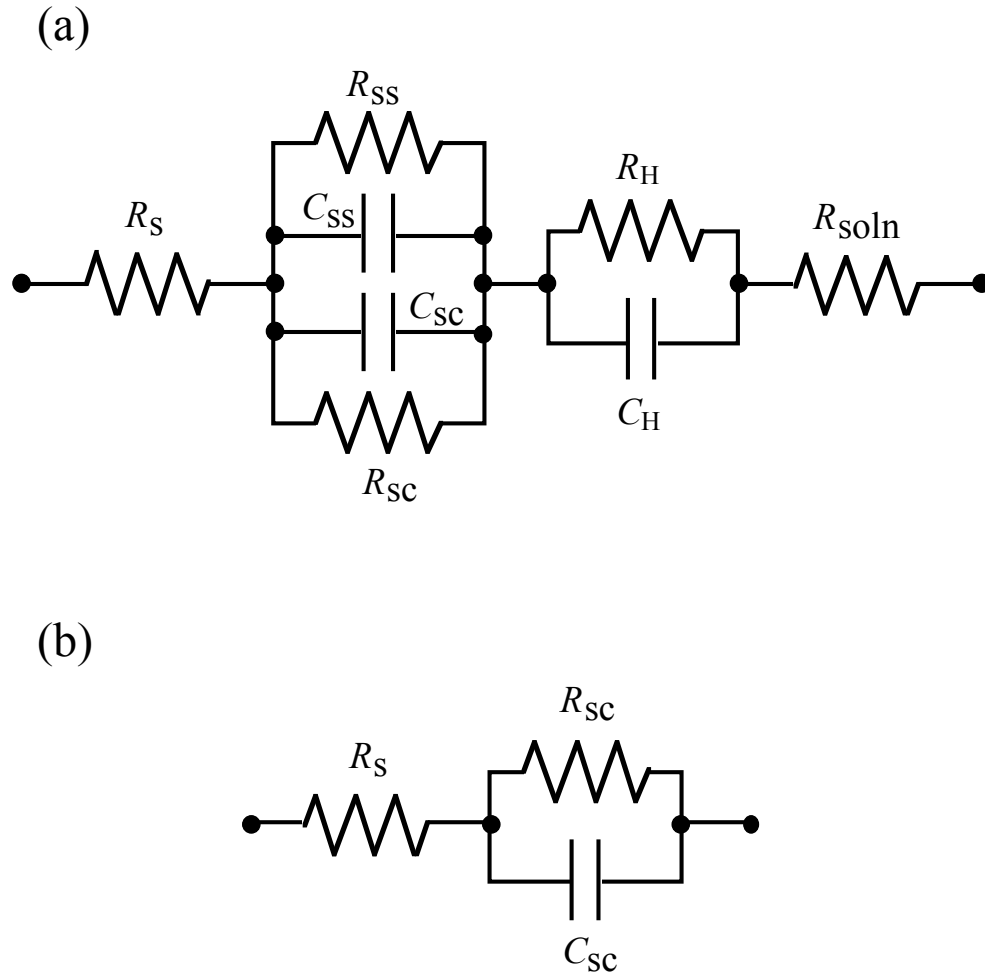


Figure 2.2

(a) A circuit of a semiconductor/liquid junction and (b) a simplified equivalent circuit of a semiconductor/liquid junction at high enough frequencies where surface states cannot react fast enough to the applied ac signal. R_s is the semiconductor bulk resistance, R_{ss} is the surface state resistance, C_{ss} is the surface state capacitance, R_{sc} is the space-charge resistance, C_{sc} is the space-charge capacitance, R_H is the Helmholtz layer resistance, C_H is the Helmholtz layer capacitance, and R_{soln} is the cell solution resistance.

3.4. Surface Analysis of *n*-GaAs in Contact with CH₃CN-CoCp₂⁺⁰ Solution

3.4.1. X-ray Photoelectron Spectroscopy

The chemistry of *n*-GaAs after exposure to CH₃CN-CoCp₂⁺⁰ solution was investigated with x-ray photoelectron spectroscopy (XPS). Immediately before the experiment all samples were etched in a N₂(g)-purged glove box using the procedure described in section 3.1. Four samples without back ohmic contacts were immersed in the following four CH₃CN solutions for 10 minutes each. Solution 1 contained 0.7 M LiClO₄, solution 2 contained 0.7 M LiClO₄ and 10 mM CoCp₂, solution 3 contained 0.7 M LiClO₄ and 10 mM CoCp₂PF₆, and solution 4 contained 0.7 M LiClO₄ and 10 mM each of both CoCp₂ and CoCp₂PF₆. In order to analyze the *n*-GaAs surfaces after electrochemical processes, customized electrodes with pre-cut glass tubing or flexible polyethylene tubing which allowed the length of these electrodes to be reduced to less than 1.5 inches were used. The electrode was immersed in an electrochemical cell with solution 4, and a potential sweep at 50 mV s⁻¹ between -0.5 and 0.3 V vs. *E*(A/A⁻) was applied for 10 minutes. All samples were rinsed with CH₃CN and sealed in vials under N₂(g).

The vials were transferred into another N₂(g)-purged glove box which is connected directly to the ultrahigh vacuum (UHV) system that houses the XPS via a high-vacuum load lock. The non-ohmic contacted GaAs samples were mounted on a stainless steel or aluminum stub with gold-plated molybdenum clips or screws. A custom-made aluminum stub designed to hold tubing down was used to mount the shortened electrodes. The tinned copper wire of the electrode was fold back to make an electrical contact with the stub. The samples stub was introduced into the load lock through a gate valve inside of the glove box. A Varian V-200 turbo pump backed by a Varian model SD-300 mechanical pump were used to evacuate the load lock to

approximately 10^{-7} Torr prior to transferring the samples into the UHV system. The XPS experiments were conducted in an M-probe surface spectrometer (Surface Science Instrument) pumped by a CTI Cryogenics-8 cryo pump. The XPS chamber was maintained at a base pressure of less than 5×10^{-10} Torr, although the operating pressure was 5×10^{-9} to 2×10^{-8} Torr. Monochromatic Al K_{α} x-rays ($h\nu = 1486.6$ eV) incident at 35° from the sample surface were used to excite electrons from the sample, while the emitted electrons were collected by a hemispherical analyzer at a take-off angle of 35° from the plane of the sample surface. Data collection and analysis were done with the M-probe package software version 3.4. The survey scan was collected in the scanned mode with an elliptical spot of dimensions $800 \mu\text{m} \times 1200 \mu\text{m}$ incident on the sample surface.

3.4.2. Cyclic Voltammetry

The possibility of surface changes when *n*-GaAs underwent electrochemical measurements in $\text{CH}_3\text{CN-LiClO}_4$ system was further investigated by the cyclic voltammetry. Cyclic voltammograms of *n*-GaAs in a standard electrolyte solution were collected using a Solartron Model 1287 potentiostat. A three-electrode potentiostatic setup was used with a SCE as the reference electrode and a large Pt as the counter electrode. The cell solution was unstirred and consists of 0.7 M LiClO_4 in CH_3CN , in the absence of a redox-active species. The data were collected from 2.0 to -2.5 V vs. SCE with a scan rate of 50 mV s^{-1} .

4. Results

4.1. Differential Capacitance vs. Potential Results and the Barrier Height of *n*-GaAs/CH₃CN-CoCp₂⁺⁰ Contacts

The barrier height of the *n*-GaAs/CH₃CN-CoCp₂⁺⁰ junction was calculated from electrochemical impedance data. The barrier height (ϕ_b) of the junction can be calculated from the V_{bi} from the following equation:⁵³

$$\phi_b = V_{bi} + \frac{kT}{q} \ln \left(\frac{N_c}{N_d} \right) \quad (2.8)$$

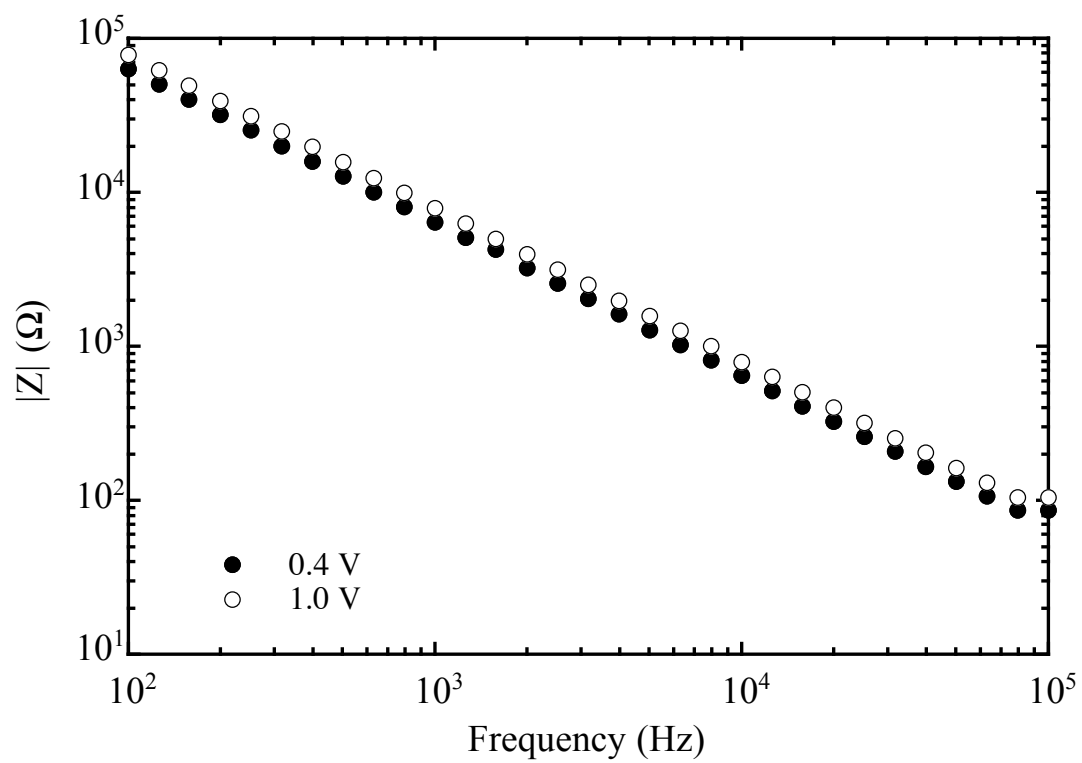
where N_c is the effective density of states in the conduction band.

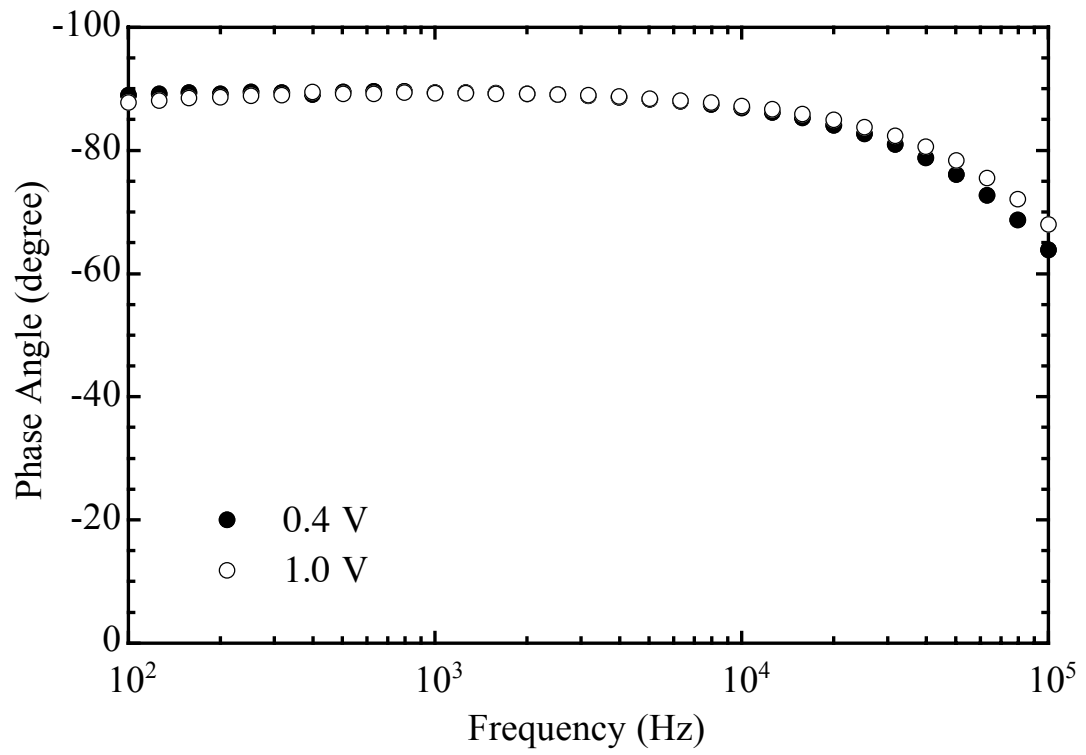
Typical representations of one set of impedance data for the *n*-GaAs/CH₃CN-CoCp₂⁺⁰ system are shown in Figure 2.3. To determine a relevant frequency range for the Mott-Schottky analysis (i.e., barrier height calculation), a plot of $\log |Z|$ vs. $\log f$ (Bode plot) and a plot of the phase angle θ vs. $\log f$ were used. A linear dependence of the total impedance on frequency (a linear region on the Bode plot) with a slope of 1 indicates the dominance of the space-charge capacitance in the circuit model illustrated in Figure 2.2b. Figure 2.3a displays the measured circuit impedance as a function of frequency in Bode plot form for a representative electrode at applied potentials of 0.40 V and 1.00 V vs. $E(A/A^-)$. For 100 Hz $< f < 50$ kHz range, the mean slope of the Bode plots between 0.40 V and 1.00 V vs. $E(A/A^-)$ was -0.995 ± 0.001 , which means that the differential capacitance was independent of the measured frequency. Another criterion for the space-charge capacitance dominance was a measured phase angle of $\approx 90^\circ$. For the work done in this chapter, only the frequencies with phase angles above 80° were used, and this frequency range was found to be between 100 Hz and 50 KHz (Figure

2.3b). During the subsequent analysis, only frequencies that yielded linear fits with $R^2 \geq 0.999$ were used to calculate the barrier height values. Figure 2.3c displays a typical Nyquist plot of the n -GaAs/CH₃CN-CoCp₂⁺⁰ interface. The R_{sc} values were very large in all cases, which again confirmed the relevance of the frequency range selected. Figure 2.4a display a Mott-Schottky plot at six different measured frequencies, and Figure 2.4b shows the extrapolated linear fits to these data. For this particular set of data, the average extrapolated x-intercept for 9 different measured frequencies was -0.740 ± 0.009 V, and using Equation 2.10, the V_{bi} was calculated to be 0.765 ± 0.009 V. From Equation 2.11, the ϕ_b of this electrode was found to be 0.902 ± 0.009 V. The mean observed Mott-Schottky plot slope of $(1.400 \pm 0.014) \times 10^{15} \text{ F}^{-2} \text{ V}^{-1}$ yielded a measured dopant density of $(1.41 \pm 0.01) \times 10^{17} \text{ cm}^{-3}$, which is in good agreement with that specified by the manufacturer. The mean barrier height calculated from 8 samples with a total of 17 trials was 0.915 ± 0.054 V and the mean calculated dopant density was $(1.16 \pm 0.15) \times 10^{17} \text{ cm}^{-3}$, which is also in good agreement with that specified by the manufacturer.

Figure 2.3

(a) A representative Bode plot (impedance $|Z|$ vs. frequency f), (b) a plot of phase angle vs. $\log f$, and (c) a Nyquist plot (Z_{im} vs. Z_{re}) for the n -GaAs/CH₃CN-CoCp₂⁺⁰ junction at an applied potential of +0.4 V vs. $E(A/A^-)$ (filled circles) and +1.0 V vs. $E(A/A^-)$ (open circles). The redox couple concentrations were $[A] = [A^-] = 10$ mM, and $E(A/A^-)$ was -0.887 V vs. SCE.

**Figure 2.3a**

**Figure 2.3b**

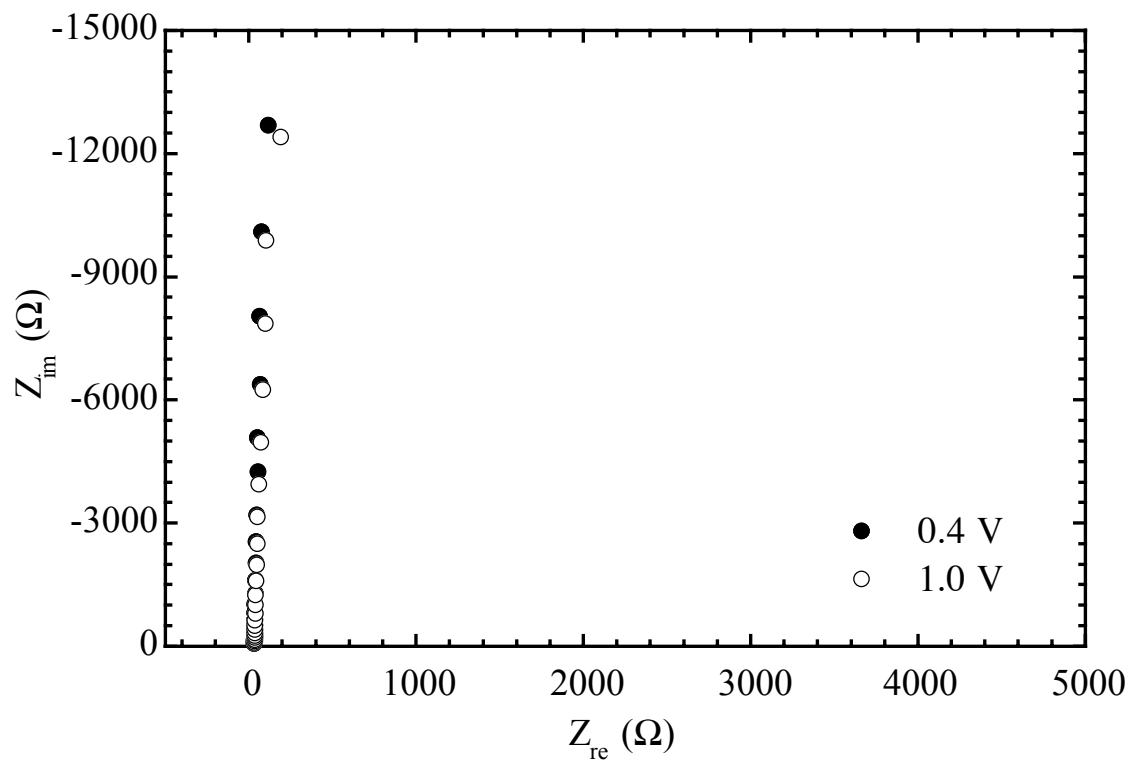
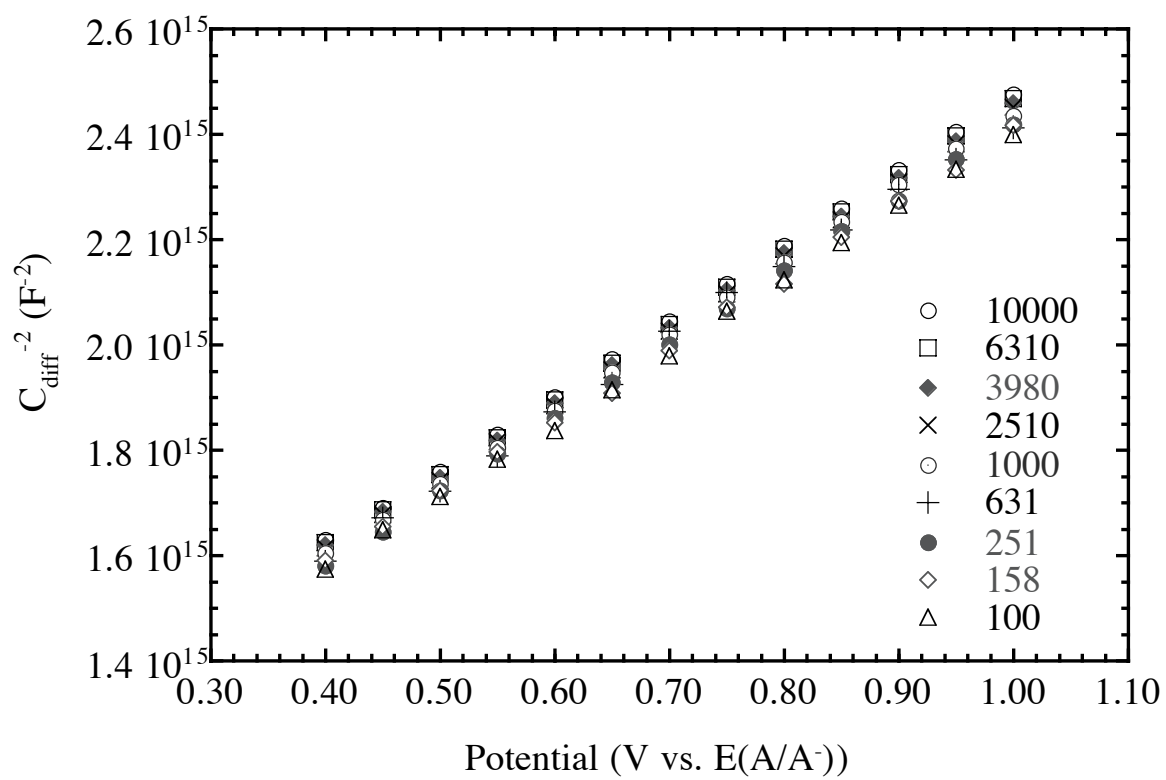
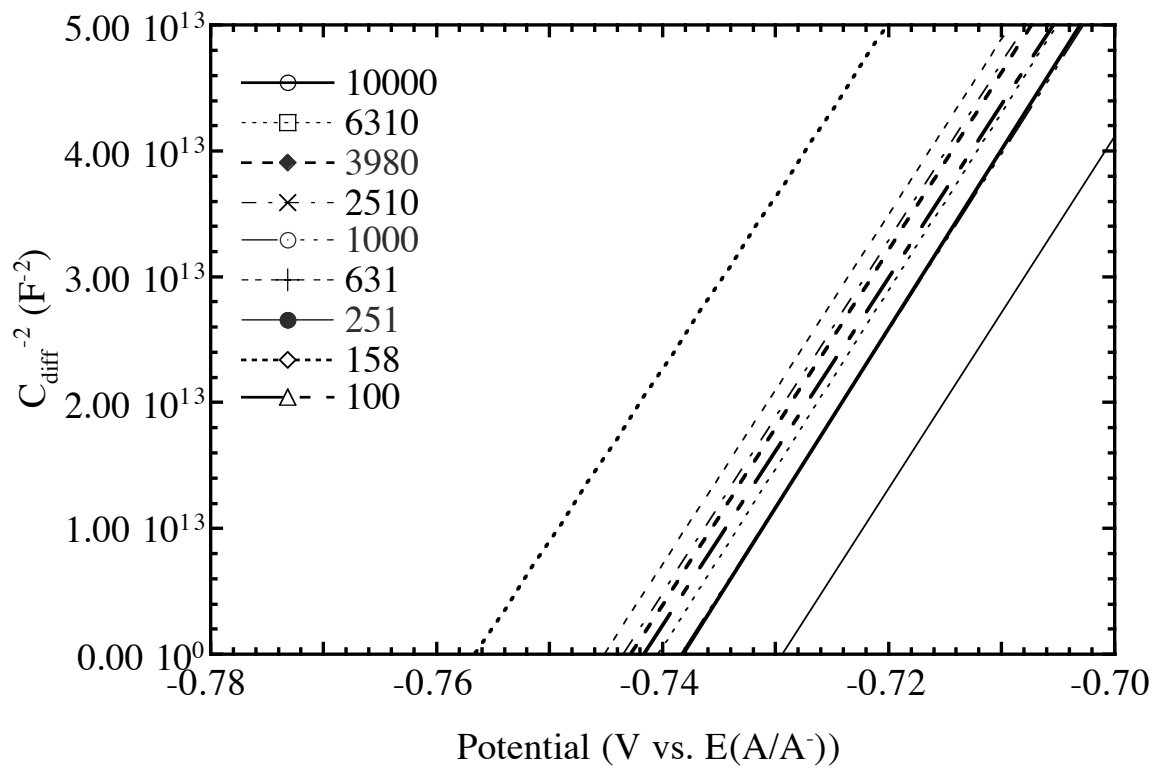


Figure 2.3c

Figure 2.4

(a) Mott-Schottky plot of the n -GaAs/CH₃CN-CoCp₂⁺⁰ junction. (b) The linear extrapolations of data shown in (a), and all linear fits yielded correlation coefficients of 0.999 or greater. The measuring frequency range shown is 100 Hz to 10 kHz. For this electrode, the ϕ_b was calculated to be 0.902 ± 0.009 V and the measured dopant density was $(1.41 \pm 0.01) \times 10^{17} \text{ cm}^{-3}$. The total cell resistance was $\sim 37 \text{ } \Omega$.

**Figure 2.4a**

**Figure 2.4b**

4.2. Steady-State $J-E$ Behavior of n -GaAs/ $\text{CH}_3\text{CN-CoCp}_2^{+/0}$ Contacts

4.2.1. $J-E$ Data for n -GaAs electrodes in $\text{CH}_3\text{CN-CoCp}_2^{+/0}$ solutions

Figure 2.5 displays a typical current density vs. potential ($J-E$) data for n -GaAs in contact with CH_3CN -10 mM CoCp_2 -10 mM CoCp_2PF_6 solution in the dark and at several different light intensities. At higher illumination intensities, typically at J_{ph} above 0.7 mA cm^{-2} , the $J-E$ curves exhibited hysteresis behavior indicating possible surface reaction. The sensitivity of the n -GaAs material on the solution quality could be observed in Figure 2.6. The $J-E$ data was collected in the same solution except that CH_3CN was distilled only once over CaH_2 , and in this case the hysteresis occurred even at lower J_{ph} values. The electrode surfaces were sometimes damaged to a point that the standard chemical etch could not repair the electrode. For this reason, an extra step was taken to distill CH_3CN over P_2O_5 after CaH_2 , and the light intensity was carefully controlled not to overexpose the electrode surfaces.

4.2.2. Photoresponses of n -GaAs electrodes in $\text{CH}_3\text{CN-CoCp}_2^{+/0}$ and $\text{CH}_3\text{CN-Fc}^{+/0}$ solutions

For n -GaAs/ $\text{CH}_3\text{CN-CoCp}_2^{+/0}$ junctions, the average calculated diode quality factor was 1.48 ± 0.08 , and the mean calculated V_{oc} value was 320 ± 14 mV at $J_{\text{ph}} = 1$ mA/ cm^2 . For n -GaAs/ $\text{CH}_3\text{CN-Fc}^{+/0}$ junctions, the average calculated diode quality factor was 1.51 ± 0.05 , and the mean calculated V_{oc} value was 718 ± 24 mV at $J_{\text{ph}} = 20$ mA/ cm^2 . The diode quality factors for both contacts are in good agreement with obtained values from prior work. The V_{oc} values observed are, however, lower than the previously observed value of 490 ± 60 mV in $\text{CH}_3\text{CN-CoCp}_2^{+/0}$ and 822 ± 4 mV in $\text{CH}_3\text{CN-Fc}^{+/0}$ at the same J_{ph} . The electrode material used for prior study was of high quality epitaxial n -GaAs samples, and this difference in semiconductor quality was perceived to cause this

discrepancy in V_{oc} values. A white-silvery film was observed on the electrode surface after each experiment in $\text{CH}_3\text{CN-CoCp}_2^{+/0}$ solution, in addition, some white-silvery powders were also observed in the cell solution after electrochemical measurements were made using several electrodes.

4.2.3. Effects of Exposure to $\text{CH}_3\text{CN-CoCp}_2^{+/0}$ Solutions on the Behavior of $n\text{-GaAs/CH}_3\text{CN-Fc}^{+/0}$ Contacts

Since $J-E$ behavior of $n\text{-GaAs}$ in contact with $\text{CH}_3\text{CN-Fc}^{+/0}$ solution was stable and reproducible. Comparing the $J-E$ curves of this junction before and after the electrode was exposed to $\text{CH}_3\text{CN-CoCp}_2^{+/0}$ solutions could help identify if surface modification took place in $\text{CoCp}_2^{+/0}$ solution. Figure 2.7a displays $J-E$ behaviors of $n\text{-GaAs/CH}_3\text{CN-Fc}^{+/0}$ contact immediately following the etching process. After the electrodes were subjected to potential scans in $\text{CH}_3\text{CN-CoCp}_2^{+/0}$ solutions, the $J-E$ data of $n\text{-GaAs/CH}_3\text{CN-Fc}^{+/0}$ contact, as displayed in Figure 2.7b, exhibited decreased forward bias current density that was roughly half of the magnitude of the original value. Slightly lowered J_{ph} values at identical illumination intensities was also observed, although the values of V_{oc} did not change by much. The decreased cathodic current suggested that the interface between the $n\text{-GaAs}$ and $\text{CH}_3\text{CN-Fc}^{+/0}$ solution was altered when the electrode was exposed to the $\text{CH}_3\text{CN-CoCp}_2^{+/0}$ solution. The results here also indicate the possibility of surface reaction between the electrode surface and the $\text{CH}_3\text{CN-CoCp}_2^{+/0}$ solution.

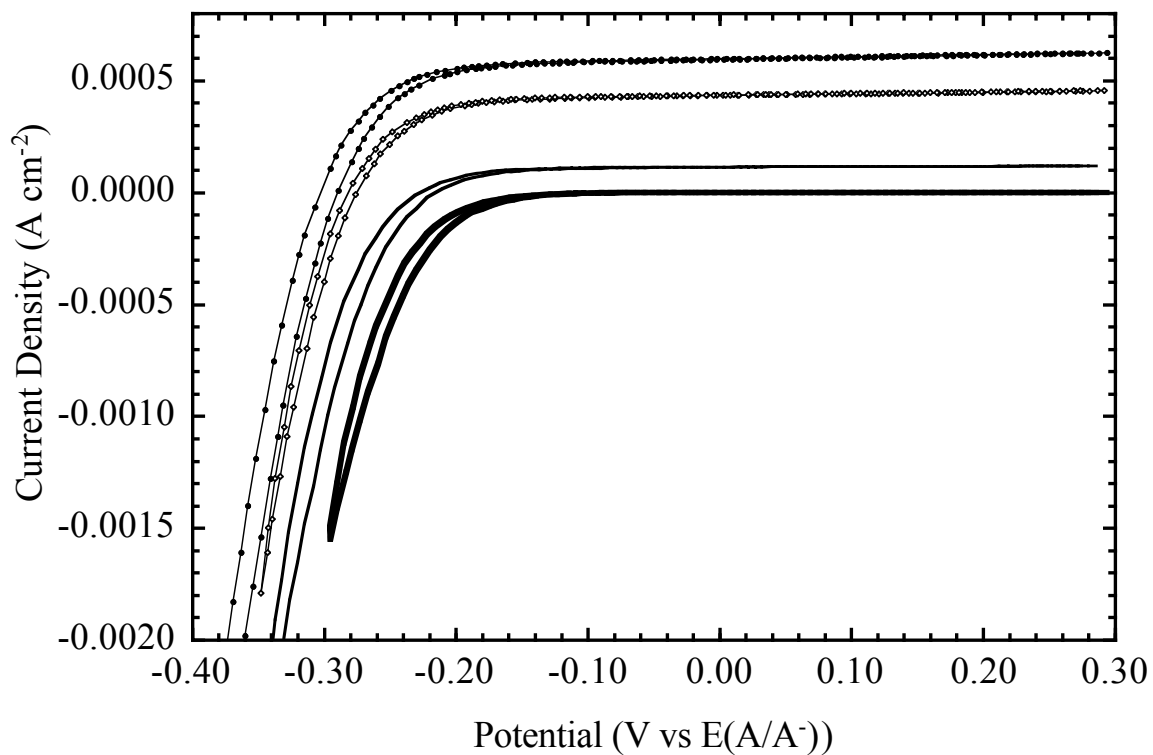


Figure 2.5

Representative J - E behaviors of n -GaAs electrodes in contact with $\text{CH}_3\text{CN-CoCp}_2^{+/0}$ solution in the dark and at three light intensities. The electrode area was 0.2661 cm^2 .

The cell solution consists of CoCp_2 (10 mM), CoCp_2PF_6 (10 mM), and LiClO_4 (0.7 M) in CH_3CN . The scan rate was 50 mV s^{-1} .

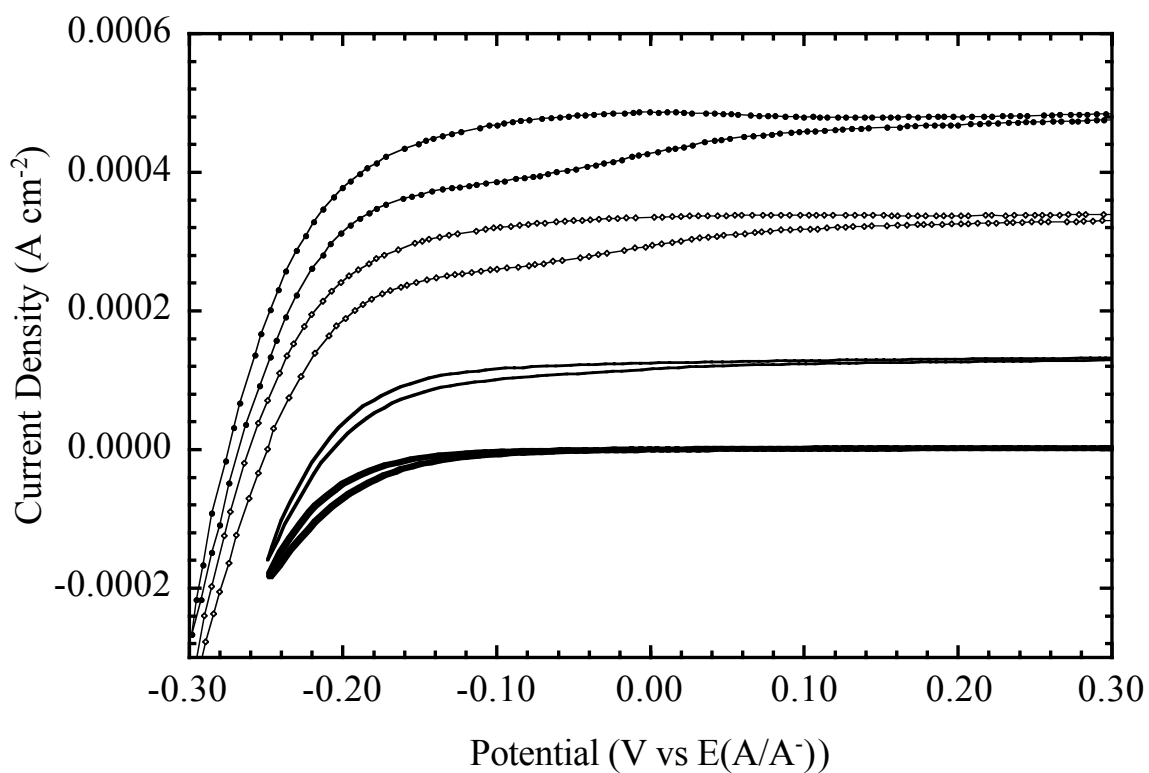


Figure 2.6

Representative J - E behaviors of n -GaAs electrodes in contact with slightly wet CH_3CN - $\text{CoCp}_2^{+/0}$ solution in the dark and at three light intensities. The electrode area was 0.2090 cm^2 . The cell solution consists of CoCp_2 (10 mM), CoCp_2PF_6 (10 mM), and LiClO_4 (0.7 M) in CH_3CN . The scan rate was 50 mV s^{-1} .

Figure 2.7

The J - E behavior of n -GaAs electrode in contact with $\text{CH}_3\text{CN-Fc}^{+/0}$ solution (a) before the electrode was used for electrochemical measurements in $\text{CH}_3\text{CN-CoCp}_2^{+/0}$ solution and (b) after performing J - E scans in $\text{CH}_3\text{CN-CoCp}_2^{+/0}$ solution in the dark and at five different light intensities from +0.2 V vs. $E(A/A^-)$ to -0.05V vs. V_{oc} . The $\text{CH}_3\text{CN-Fc}^{+/0}$ solution consists of Fc (90 mM), FcBF_4 (0.5 mM), and LiClO_4 (0.7 M) in CH_3CN , and $E(A/A^-)$ was +0.209 V vs. SCE. The $\text{CH}_3\text{CN-CoCp}_2^{+/0}$ solution consists of CoCp_2 (10 mM), CoCp_2PF_6 (10 mM), and LiClO_4 (0.7 M) in CH_3CN , and $E(A/A^-)$ was -0.888 V vs. SCE. The scan rate for both was 50 mV s^{-1} .

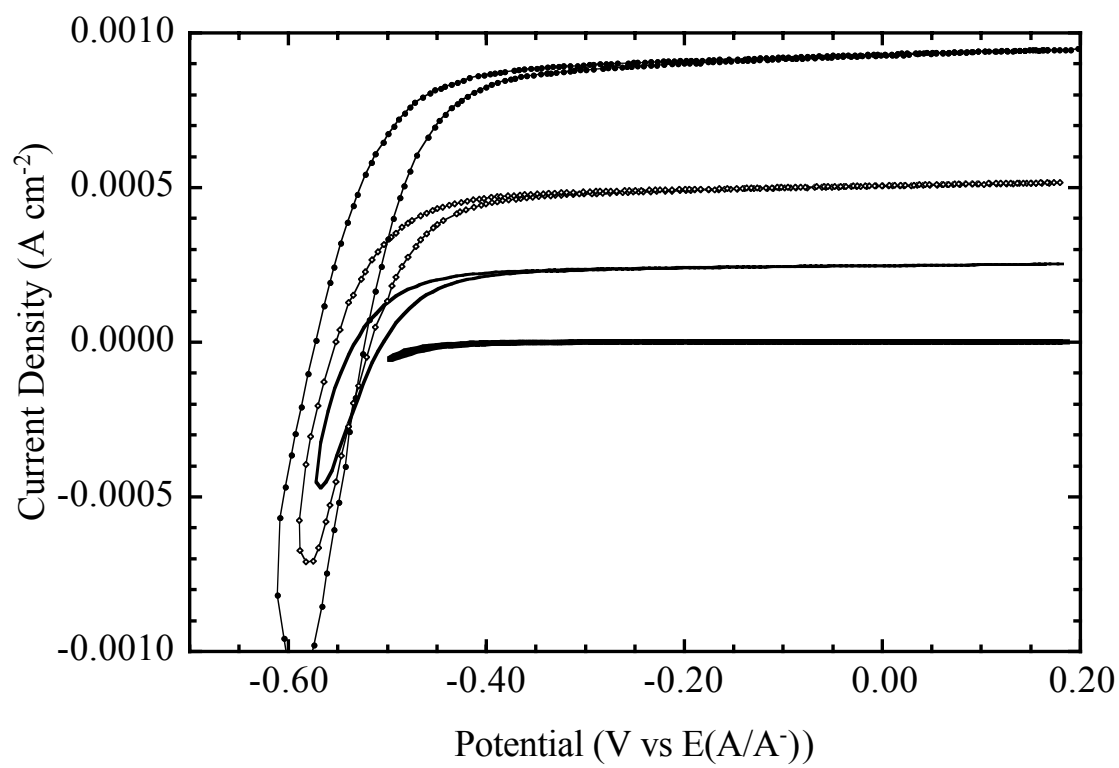
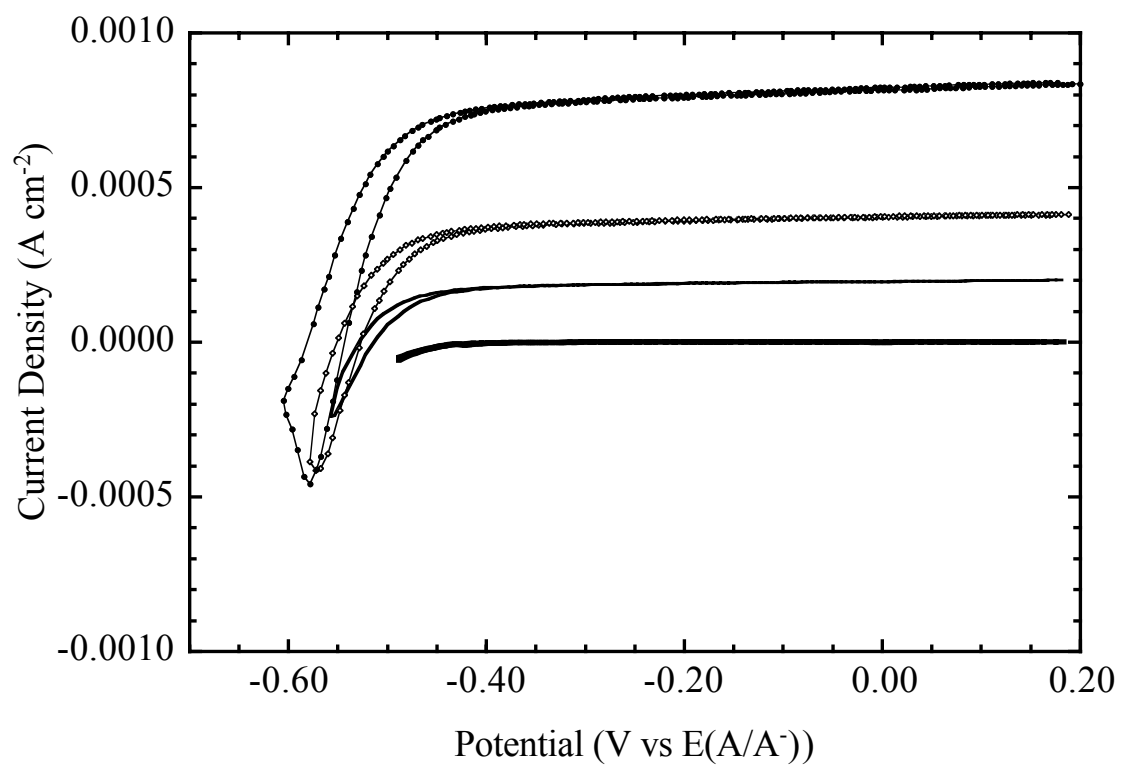


Figure 2.7a

**Figure 2.7b**

4.3. X-Ray Photoelectron Spectroscopy and Cyclic Voltammetry Data of *n*-GaAs Surfaces in Contact with the CH₃CN-CoCp₂⁺⁰ Electrolyte

The anomalous open-circuit photovoltages observed when *n*-GaAs was immersed in CH₃CN-CoCp₂⁺⁰ solution signals the presence of a chemical reaction between the *n*-GaAs and the contacting solution under the conditions explored in this work. This hypothesis was confirmed by XPS studies of the surface of *n*-GaAs electrodes before and after being exposed to the CH₃CN-CoCp₂⁺⁰ electrolyte.

Figure 2.8 depicts the XPS survey spectrum for an *n*-GaAs surface before exposure to a CH₃CN-CoCp₂⁺⁰ solution (top spectrum). Inspection of the As 3p and Ga 3d regions in high resolution mode indicated that the As peak displayed negligible contribution from excess elemental As, as has been observed previously for *n*-GaAs surfaces exposed to the KOH and Br₂-CH₃OH sequential etching process.^{44,54,55} The XP spectrum has been shown to remain unchanged after immersion or electrochemical operation of *n*-GaAs electrodes in the CH₃CN-Fc⁺⁰ electrolyte.^{44,54,55} In contrast, the XPS data of an *n*-GaAs electrode recorded after 10 minutes of *J-E* scans in a CH₃CN-CoCp₂⁺⁰ solution (bottom spectrum in Figure 2.8) looks very different from that of a clean GaAs surface. Peaks for C and O were seen but Ga and most of As peaks disappeared, no peaks for Co were observed. However, it was found that simple immersion of the *n*-GaAs in all four electrolyte solutions without undergoing electrochemical measurement (as described in section 3.4.1) did not cause observable surface modification in the XPS study. Upon removal of the electrode after 10 minutes of immersion without potential scan, no film was observed on the surfaces.

The presence of changes in the GaAs surface chemistry at negative potentials in CH₃CN was also confirmed by investigating the cyclic voltammetry of *n*-GaAs in CH₃CN-0.7 M LiClO₄ solution, in the absence of redox-active species. As displayed in Figure 2.9, a reduction wave was observed at -1.5 V vs. SCE. Because the operating

limit of the solvent/electrolyte window is < -2.5 V vs. SCE, this reduction wave must be associated with chemical changes in the surface of the GaAs electrode. This observation is in excellent agreement with prior work by Kohl and Bard, who observed similar behavior for *n*-GaAs electrodes in contact with CH_3CN -0.1 M tetra-*n*-butylammonium perchlorate (TBAP) solution.⁴¹

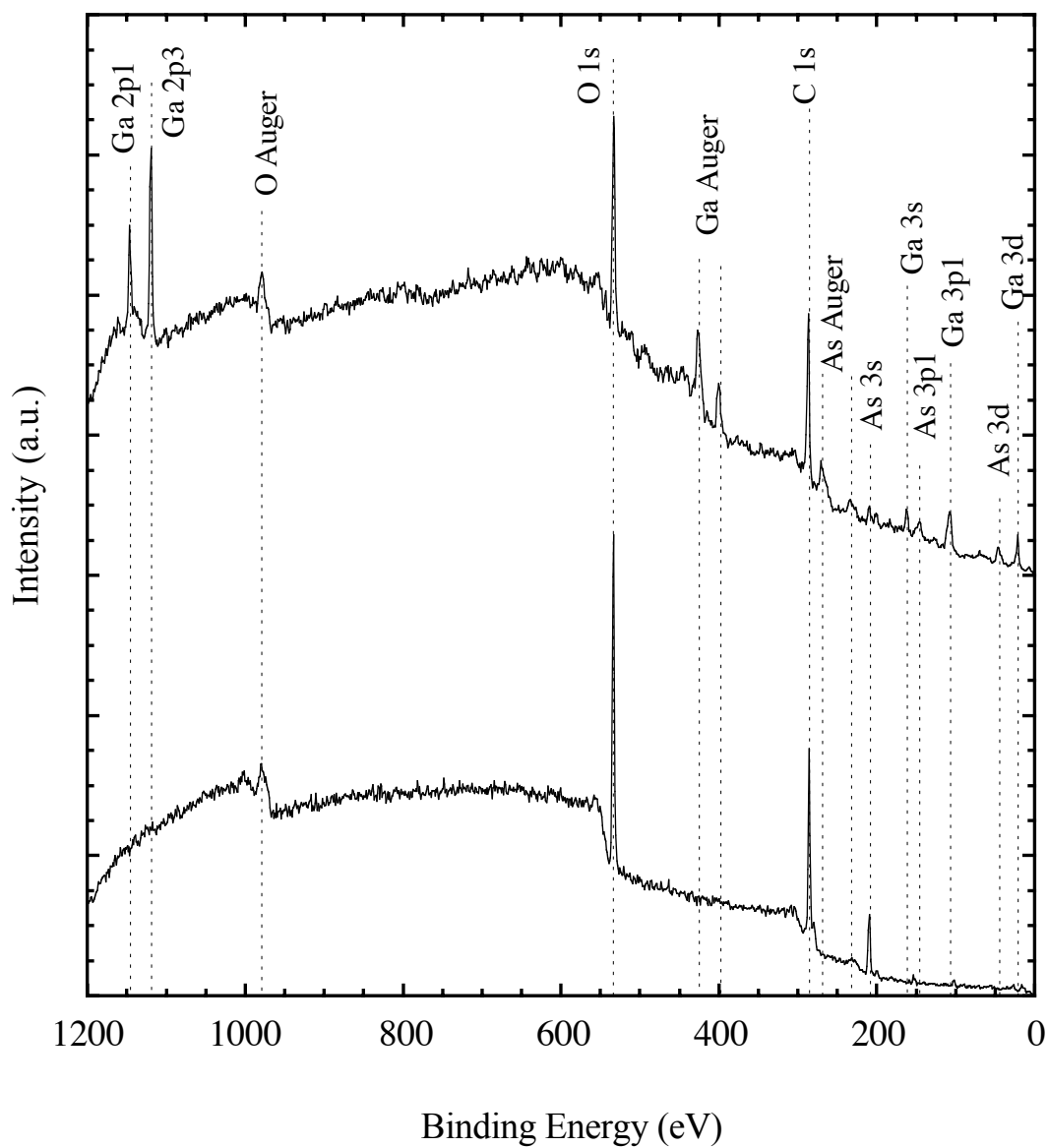


Figure 2.8

XP survey spectra of an *n*-GaAs electrode (a) immediately following etching process and (b) after 10 minutes of *J*-*E* scans in a CH₃CN solution containing LiClO₄ (0.7 M), CoCp₂PF₆ (10 mM), and CoCp₂ (10 mM).

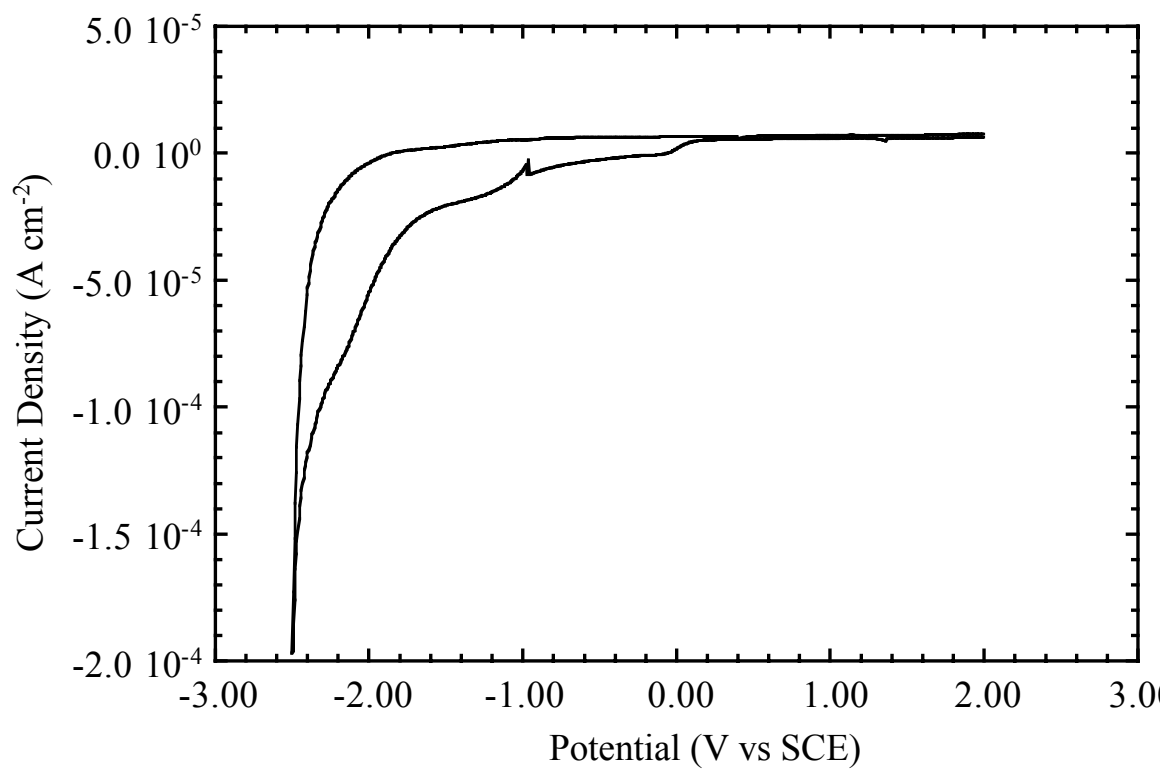


Figure 2.9

Cyclic voltammogram of *n*-GaAs in CH₃CN-0.7 M LiClO₄ in the absence of a redox species. A reduction wave at -1.5 V vs. SCE confirmed the presence of irreversible surface changes at negative potentials in CH₃CN. The scan rate was 50 mV s⁻¹.

5. Discussions

5.1. Electrochemical Properties of *n*-GaAs/CH₃CN Contacts

It is clear that *n*-GaAs electrodes exhibit partial Fermi-level pinning in contact with CH₃CN over a wide range of redox potentials. In prior work, the Fermi-level pinning behavior had been probed through the use of steady-state J - E and V_{oc} vs. T data.³³ The band edge shifts documented were often difficult to resolve when a small potential range is explored, but such behavior was clearly seen with a large variation in $E(A/A^-)$.

These conclusions are also consistent with differential capacitance measurements of the band edge positions of *n*-GaAs/CH₃CN contacts. Prior studies of the *n*-GaAs/CH₃CN-Fc⁺⁰ contact have yielded a barrier height of 1.1 V for this system,⁹ in which the Nernstian solution potential, $E(A/A^-)$, was +0.32 V vs. SCE. For comparison, Mott-Schottky measurements of the *n*-GaAs/CH₃CN-CoCp₂⁺⁰ contact indicate a barrier height of 0.92 V, even though the redox potential of these solutions is -0.9 V vs. SCE. The fact that the barrier height changed by less than 300 mV for a change of more than 1.2 V in the redox potential of the solution clearly indicates the presence of Fermi-level pinning for these *n*-GaAs/CH₃CN contacts.

Similar conclusions regarding Fermi-level pinning of GaAs electrodes in contact with non-aqueous solvents have been reached previously from cyclic voltammetric and/or impedance studies of GaAs/CH₃CN contacts.^{22,25,26,31,41,56} The cyclic voltammetric study described in this chapter has explored an even wider potential range than was investigated in the previous J - E experiments. Kohl and Bard reported the photoelectrochemical behavior of *n*-GaAs in CH₃CN solutions with a range of redox couples, including photovoltages for some redox couples having formal potentials negative of the GaAs flat-band potential.⁴¹ The ability to generate a photovoltage at the

most negative cell potentials was attributed to the pinning of the Fermi level by surface states. The current-voltage properties of the *n*-GaAs/tetrahydrofuran system were characterized using cyclic voltammetry by DiQuarto and Bard.⁵⁶ Saturation of the photovoltage at cell potentials negative of the valence band for *n*-GaAs and positive of the conduction band for *p*-GaAs was interpreted as indicating Fermi-level pinning due to either a high density of surface states or carrier inversion at the interface. Yeh and Hackerman³¹ investigated the behavior of the *n*-GaAs/N,N-dimethylformamide interface. Using cyclic voltammetry in solutions of various redox couples, they observed negative shifts in the oxidation/reduction wave of benzoquinone at *n*-GaAs under illumination as compared to the values of these peaks in the dark, and ascribed this behavior to non-ideality in the GaAs/liquid junction.

The Fermi-level pinning behavior observed herein is also consistent with a variety of prior studies of GaAs surface chemistry in other ambient. For example, non-ideal energetic behavior has been observed for *n*-GaAs surfaces exposed to a variety of impurities in UHV, with formation of As defects or excess elemental As thought to be the source of the persistent Fermi-level pinning of *n*-GaAs surfaces.⁵⁷⁻⁵⁹ In addition, formation of metal contacts on *n*-GaAs is well documented to result in Fermi-level pinning.^{53,60,61} In fact, we are not aware of any series of *n*-GaAs contacts reported to date in which Fermi-level pinning has not been observed when the electrochemical potential of the contacting phase has been varied over a significant range.

5.2. Interfacial Rate Constant Determinations Using *n*-GaAs/CH₃CN Contacts

The XPS analysis of the GaAs system shows the formation of a carbonaceous overlayer on the GaAs surface subsequent to electrochemical measurements in the CH₃CN-CoCp₂⁺⁰ solution. The evidence for this irreversible surface changes implies that a significant portion of the interfacial current in the *n*-GaAs/CH₃CN-CoCp₂⁺⁰ contact

flows through pathways that do not involve the direct transfer of electrons from the conduction band of the semiconductor into dissolved, nonadsorbed redox acceptor species. The XPS data clearly indicate that a chemical reaction, which produces a carbonaceous surface film, dominates the interfacial chemistry of the *n*-GaAs/CH₃CN-CoCp₂⁺⁰ contact at potentials sufficiently negative to produce cathodic current flow through the interfaces. This film might introduce surface states and thereby raise the overall flux, act as an insulator and block the interfacial current from flowing, or both. The presence of such a film also implies that the concentration of adsorbed electroactive CoCp₂⁺⁰-based sites can not be directly deduced under these experimental conditions from mass-change measurements of the electrode.

The *n*-GaAs electrodes investigated in this chapter and prior work exhibited higher open-circuit voltages, and therefore must have lower values of k_{et} than have been reported for *n*-GaAs electrodes exposed to less optimal etching procedures.⁷ Since the rate constant k_{et} describes the direct transfer of electrons from the conduction band of the semiconductor to nonadsorbing electron acceptor ions in the solution phase, k_{et} can not depend on the surface condition or etching procedure. The photovoltage value observed at $J_{\text{ph}} = 1 \text{ mA cm}^{-2}$ can therefore be used to set an upper bound on k_{et} for the *n*-GaAs/CH₃CN-CoCp₂⁺⁰ system, because the rate of the direct electron-transfer process is equal to, or less than, the observed interfacial charge transfer flux. This produces an upper bound on k_{et} for the *n*-GaAs/CH₃CN-CoCp₂⁺⁰ contact of less than $10^{-14} \text{ cm}^4 \text{ s}^{-1}$, which is consistent with theoretical expectations for such process.^{4,6,11} It is, of course, always possible to produce less rectifying contacts through introduction of etch-induced surface defects or surface nonstoichiometries. However, regardless of the surface condition, etch-related increases in current density at a given electrode potential are a clear indication that the direct electron-transfer process is not being measured from the interfacial current densities observed at such contacts.

Additional evidence supporting the presence of surface-states at the *n*-GaAs/CH₃CN-CoCp₂⁺⁰ contact can be obtained by comparison of the *J-E* properties of the *n*-GaAs/CH₃CN-CoCp₂⁺⁰ contact with those of the *n*-GaAs/CH₃CN-Fc⁺⁰ contact. The results had shown that the surface-state recombination is the dominant recombination mechanism for the *n*-GaAs/CH₃CN-Fc⁺⁰ semiconductor/liquid contact, and thermionic emission is greatly suppressed in this system.³³ Thus the value of k_{et} must be smaller than $10^{-14} \text{ cm}^4 \text{ s}^{-1}$ for the *n*-GaAs/CH₃CN-Fc⁺⁰ contact in order to have the observed flux dominate the recombination current of the contact.⁹ Because the barrier heights are so similar between the *n*-GaAs/CH₃CN-CoCp₂⁺⁰ and *n*-GaAs/CH₃CN-Fc⁺⁰ contacts, and the Marcus nuclear reorganization energy term is only weakly dependent on the driving force for the expected reorganization energy of between 0.5 and 1.0 eV for these metallocenes at semiconductor electrodes having this value of the barrier height,^{4,11,62,63} the charge-transfer rate constants should certainly not differ by more than a factor of 10^2 . This comparison therefore also supports the notion that surface states, and not direct interfacial electron transfer, dominate the interfacial kinetics of the *n*-GaAs/CH₃CN-CoCp₂⁺⁰ contact. The discovery of chemical methods to remove this Fermi-level pinning condition, and subsequent demonstration of an ideal energetic barrier height vs. $E(A/A^-)$ dependence as well as the expected second-order kinetic rate law, are therefore required before robust k_{et} values can be extracted from the steady-state *J-E* behavior of *n*-GaAs/CH₃CN contacts.

6. Summary

The barrier height of n -GaAs/CH₃CN-CoCp₂⁺⁰ interface has been measured, and combined with prior barrier height result for n -GaAs/CH₃CN-Fc⁺⁰ interface,⁹ the presence of partial Fermi-level pinning was confirmed. The presence of irreversible chemical and/or electrochemical changes on n -GaAs electrodes immersed in CH₃CN-CoCp₂⁺⁰ solutions was investigated using x-ray photoelectron spectroscopy (XPS), steady-state current density–potential (J – E) measurements, and cyclic voltammetric studies that were designed to probe surface reactions. Since the dominant recombination mechanism of n -GaAs/CH₃CN interfaces is surface-state recombination and not direct electron transfer, the k_{et} value could not be evaluated from the steady-state J – E data of n -GaAs/CH₃CN-CoCp₂⁺⁰ junction. The similarity in barrier heights of n -GaAs/CH₃CN-CoCp₂⁺⁰ and n -GaAs/CH₃CN-Fc⁺⁰ junctions indicated that the charge-transfer rate constants should not differ by more than a factor of 10². Only when an ideal energetic barrier height vs. $E(A/A^-)$ dependence and the second-order rate law can be established, a robust k_{et} values can then be extracted from this system.

7. Acknowledgments

This work was supported by the U.S. Department of Energy (Office of Basic Energy Sciences) and the Eastman Kodak Company.

8. References and Notes

- (1) Diol, S. J.; Poles, E.; Rosenwaks, Y.; Miller, R. J. D. *J. Phys. Chem. B* **1998**, *102*, 6193.
- (2) Fan, F. R.; Bard, A. J. *J. Phys. Chem.* **1991**, *95*, 1969.
- (3) Kesselman, J.; Hoffman, M. R.; Shreve, G. A.; Lewis, N. S. *J. Phys. Chem.* **1995**, *98*, 13385.
- (4) Lewis, N. S. *Ann. Rev. Phys. Chem.* **1991**, *42*, 543.
- (5) Lewis, N. S. *Sol. Energy Mater. Sol. Cells* **1995**, *38*, 323.
- (6) Lewis, N. S. *J. Phys. Chem. B* **1998**, *102*, 4843.
- (7) Meier, A.; Kocha, S. S.; Hanna, M. C.; Nozik, A. J.; Siemoneit, K.; Reineke-Koch, R.; Memming, R. *J. Phys. Chem. B* **1997**, *101*, 7038.
- (8) Meier, A.; Selmarten, D. C.; Siemoneit, K.; Smith, B. B.; Nozik, A. J. *J. Phys. Chem. B* **1999**, *103*, 2122.
- (9) Pomykal, K. E.; Fajardo, A. M.; Lewis, N. S. *J. Phys. Chem.* **1996**, *100*, 3652.
- (10) Pomykal, K. E.; Lewis, N. S. *J. Phys. Chem. B* **1997**, *101*, 2476.
- (11) Royea, W. J.; Fajardo, A. M.; Lewis, N. S. *J. Phys. Chem. B* **1998**, *102*, 3653.
- (12) Sinn, C.; Meisser, D.; Memming, R. *J. Electrochem. Soc.* **1990**, *137*, 168.
- (13) Wang, D.; Buontempo, J.; Li, Z. W.; Miller, R. J. D. *Chem. Phys. Lett.* **1995**, *232*, 7.
- (14) Fajardo, A. M.; Lewis, N. S. *Spectrum* **1997**, *10*, 1.
- (15) Fajardo, A. M.; Lewis, N. S. *Science* **1996**, *274*, 969.
- (16) Fajardo, A. M.; Lewis, N. S. *J. Phys. Chem. B* **1997**, *101*, 11136.
- (17) Horrocks, B. R.; Mirkin, M. V.; Bard, A. J. *J. Phys. Chem.* **1994**, *98*, 9106.
- (18) Rosenwaks, Y.; Thacker, B. R.; Ahrenkiel, R. K.; Nozik, A. J. *J. Phys. Chem.* **1992**, *96*, 10096.
- (19) Rosenwaks, Y.; Thacker, B. R.; Nozik, A. J.; Ellingson, R. J.; Burr, K. C.; Tang, C. L. *J. Phys. Chem.* **1994**, *98*, 2739.
- (20) Smith, B. B.; Halley, J. W.; Nozik, A. J. *Chem. Phys.* **1996**, *205*, 245.
- (21) Bard, A. J.; Bocarsly, A. B.; Fan, F. R. F.; Walton, E. G.; Wrighton, M. S. *J. Am. Chem. Soc.* **1980**, *102*, 3671.
- (22) Nagasubramanian, G.; Wheeler, B. L.; Bard, A. J. *J. Electrochem. Soc.* **1983**, *130*, 1680.
- (23) Singh, P.; Rajeshwar, K. *J. Electrochem. Soc.* **1981**, *128*, 1724.

- (24) Singh, P.; Rajeshwar, K.; DuBow, J.; Job, R. *J. Am. Chem. Soc.* **1980**, *102*, 4676.
- (25) Ba, B.; Fotouhi, B.; Gabouze, N.; Gorochoy, O.; Cachet, H. *J. Electroanal. Chem.* **1992**, *334*, 263.
- (26) Gabouze, N.; Fotouhi, B.; Gorochoy, O.; Cachet, H.; Yao, N. A. *J. Electroanal. Chem.* **1987**, *237*, 289.
- (27) Salvador, P.; Diez, Y. G.; Soto, L. G. *Surf. Sci.* **1991**, *245*, 324.
- (28) Uosaki, K.; Shigematsu, Y.; Kaneko, S.; Kita, H. *J. Phys. Chem.* **1989**, *93*, 6521.
- (29) DiQuarto, F.; Bard, A. J. *J. Electroanal. Chem.* **1981**, *127*, 43.
- (30) Langmuir, M. E.; Hoenig, P.; Rauh, R. D. *J. Electrochem. Soc.* **1981**, *128*, 2357.
- (31) Yeh, L.-S. R.; Hackerman, N. *J. Phys. Chem.* **1978**, *82*, 2719.
- (32) Tufts, B. J.; Casagrande, L. G.; Lewis, N. S.; Grunthaner, F. J. *Appl. Phys. Lett.* **1990**, *57*, 2262.
- (33) Casagrande, L. G.; Lewis, N. S. *J. Am. Chem. Soc.* **1985**, *107*, 5793.
- (34) Morrison, S. R. *Electrochemistry at Semiconductor and Oxidized Metal Electrodes*; Plenum: New York, 1980.
- (35) Casagrande, L. G. Ph.D., Stanford University, 1988.
- (36) Howard, J. N.; Koval, C. A. *Anal. Chem.* **1994**, *66*, 4525.
- (37) Gerischer, H. *J. Phys. Chem.* **1991**, *95*, 1356.
- (38) Evenor, M.; Huppert, D.; Gottesfeld, S. *J. Electrochem. Soc.* **1986**, *133*, 296.
- (39) Chazalviel, J.-N. *J. Electrochem. Soc.* **1982**, *129*, 963.
- (40) Kohl, P. A.; Bard, A. J. *J. Electrochem. Soc.* **1979**, *126*, 603.
- (41) Kohl, P. A.; Bard, A. J. *J. Electrochem. Soc.* **1979**, *126*, 59.
- (42) Lin, M. S.; Hung, N.; Wrighton, M. S. *J. Electroanal. Chem.* **1983**, *149*, 27.
- (43) Casagrande, L. G. Ph.D. Thesis, Stanford University, 1988.
- (44) Bansal, A.; Tan, M. X.; Tufts, B. J.; Lewis, N. S. *J. Phys. Chem.* **1993**, *97*, 7309.
- (45) Casagrande, L. G.; Tufts, B. J.; Lewis, N. S. *J. Phys. Chem.* **1991**, *95*, 1373.
- (46) Stocker, H. J.; Aspnes, D. E. *Appl. Phys. Lett.* **1983**, *42*, 85.
- (47) Vasquez, R. P.; Lewis, B. F.; Frunthaner, F. J. *J. Vac. Sci. Technol.* **1983**, *B1*, 791.
- (48) Hendrickson, D. H.; Sohn, Y. S.; Gray, H. B. *Inorg. Chem.* **1971**, *10*, 1559.
- (49) Sheats, J. E.; Rausch, M. D. *J. Org. Chem.* **1970**, *35*, 3245.
- (50) CAUTION: Lithium perchlorate reacts explosively with organics at these temperatures. Great care must be taken to ensure that no organic material is exposed to the molten salt. Lithium perchlorate also decomposes at temperatures above 400 °C, therefore the molten salt temperature must be kept below this value.

- (51) Bard, A. J.; Faulkner, L. R. *Electrochemical Methods: Fundamentals and Applications*; John Wiley & Sons: New York, 1980.
- (52) Tan, M. X.; Laibinis, P. E.; Nguyen, S. T.; Kesselman, J. M.; Stanton, C. E.; Lewis, N. S. *Prog. Inorg. Chem.* **1994**, *41*, 21.
- (53) Sze, S. M. *The Physics of Semiconductor Devices*; 2nd ed.; Wiley: New York, 1981.
- (54) Lunt, S. R.; Casagrande, L. G.; Tufts, B. J.; Lewis, N. S. *J. Phys. Chem.* **1988**, *92*, 5766.
- (55) Tufts, B. J.; Abrahams, I. L.; Caley, C. E.; Lunt, S. R.; Miskelly, G. M.; Sailor, M. J.; Santangelo, P. G.; Lewis, N. S.; Roe, A. L.; Hodgson, K. O. *J. Am. Chem. Soc.* **1990**, *112*, 5123.
- (56) DiQuarto, F.; Bard, A. J. *J. Electroanal. Chem.* **1981**, *127*, 43.
- (57) Spindt, C. J.; Liu, D.; Miyano, K.; Meissner, P. L.; Chiang, T. T.; Kendelewicz, T.; Lindau, I.; Spicer, W. E. *Appl. Phys. Lett.* **1989**, *55*, 861.
- (58) Spicer, W. E.; Chye, P. W.; Skeath, P. R.; Su, C. Y.; Lindau, I. *J. Vac. Sci. Technol.* **1979**, *16*, 1422.
- (59) Spicer, W. E.; Lindau, I.; Skeath, P.; Su, C. Y. *J. Vac. Sci. Technol.* **1980**, *17*, 1019.
- (60) Mead, C. A.; Spitzer, W. G. *Phys. Rev.* **1964**, *134*, A713.
- (61) McGill, T. C. *J. Vac. Sci. Technol.* **1974**, *11*, 935.
- (62) Uhlendorf, I.; Reineke-Koch, R.; Memming, R. *J. Phys. Chem.* **1996**, *100*, 4930.
- (63) Fonash, S. J. *Solar Cell Device Physics*; Academic: New York, 1981.